Biophysical *Journal*
Article

Biophysical Society

Multistep Changes in Amyloid Structure Induced by Cross-Seeding on a Rugged Energy Landscape

Keisuke Yuzu,[1] Naoki Yamamoto,[2] Masahiro Noji,[3,4] Masatomo So,[3] Yuji Goto,[3,5] Tetsushi Iwasaki,[1,6] Motonari Tsubaki,[1] and Eri Chatani[1,*]

[1]Graduate School of Science, Kobe University, Kobe, Hyogo, Japan; [2]School of Medicine, Jichi Medical University, Shimotsuke, Tochigi, Japan; [3]Institute for Protein Research, Osaka University, Suita, Osaka Japan; [4]Graduate School of Human and Environmental Studies, Kyoto University, Yoshidanihonmatsu, Kyoto, Japan; [5]Global Center for Medical Engineering and Informatics, Osaka University, Suita, Osaka, Japan; and [6]Biosignal Research Center, Kobe University, Kobe, Hyogo, Japan

ABSTRACT Amyloid fibrils are aberrant protein aggregates associated with various amyloidoses and neurodegenerative diseases. It is recently indicated that structural diversity of amyloid fibrils often results in different pathological phenotypes, including cytotoxicity and infectivity. The diverse structures are predicted to propagate by seed-dependent growth, which is one of the characteristic properties of amyloid fibrils. However, much remains unknown regarding how exactly the amyloid structures are inherited to subsequent generations by seeding reaction. Here, we investigated the behaviors of self- and cross-seeding of amyloid fibrils of human and bovine insulin in terms of thioflavin T fluorescence, morphology, secondary structure, and iodine staining. Insulin amyloid fibrils exhibited different structures, depending on species, each of which replicated in self-seeding. In contrast, gradual structural changes were observed in cross-seeding, and a new type of amyloid structure with distinct morphology and cytotoxicity was formed when human insulin was seeded with bovine insulin seeds. Remarkably, iodine staining tracked changes in amyloid structure sensitively, and singular value decomposition analysis of the ultraviolet-visible absorption spectra of the fibril-bound iodine has revealed the presence of one or more intermediate metastable states during the structural changes. From these findings, we propose a propagation scheme with multistep structural changes in cross-seeding between two heterologous proteins, which is accounted for as a consequence of the rugged energy landscape of amyloid formation.

SIGNIFICANCE We have examined how fibril structure is propagated by cross-seeding (i.e., a seeding reaction between two proteins with heterologous sequences), which is considered to play an important role in the transmission and progression of the amyloid-related diseases. By using human and bovine insulin as model proteins, we have found that cross-seeding causes gradual amyloid structural changes from original seeds, and in some cases, a new-type amyloid structure with distinct morphology and cytotoxicity is formed. Based on the results of singular value decomposition analysis of ultraviolet-visible absorption spectra of iodine-stained insulin fibrils, the conformational changes are explained as a multistep transition with intermediate metastable states, suggesting the rough energy landscape of amyloid formation with local minima.

INTRODUCTION

Protein misfolding induces aberrant aggregation and often results in the formation of amyloid fibrils that are associated with more than 40 amyloidoses and neurodegenerative diseases, including Alzheimer's and Parkinson's diseases (1–4). Although needle-like morphology and cross-β structure are common basic properties of amyloid fibrils, it has been revealed that amyloid fibrils show microscopic structural diversity (4–6). Differences in amyloid structure are observed even when the amino acid sequence is identical or very similar, and details of these different structures have recently been clarified at an atomic level owing to the progress of cryo-electron microscopy (7,8) and solid-state NMR spectroscopy (9,10). Variations of amyloid structure often lead to various physicochemical properties, such as morphology (11,12) and structural stability (13). Moreover, it has also been suggested that such structure-dependent properties of amyloid fibrils exert diverse

Submitted September 10, 2020, and accepted for publication December 10, 2020.

*Correspondence: chatani@crystal.kobe-u.ac.jp

Editor: James Shorter.

https://doi.org/10.1016/j.bpj.2020.12.005

pathological effects in vivo (7,8,14–16), and researches on relationships between amyloid fibril structure and its phenotype have been conducted vigorously. In prion disease, which has been revealed as an infectious amyloidosis, it is proposed that the diverse structures of prion fibrils result in different transmissibility (13). Amyloid conformations are thus an important factor for determining various physiological phenotypes and now attract much attention for understanding pathology based on protein structure.

According to a nucleation-dependent polymerization, which is the basic model of amyloid assembly, the growth of amyloid fibrils is accelerated by the presence of fibril seeds (17). With this mechanism, diverse structures of amyloid fibrils are proposed to proliferate in vivo and therefore to play an important role in the transmission and progression of diseases. Typically, seed-dependent elongation with the same proteins (i.e., self-seeding) occurs most preferably, and in this case, the structure of seeds is replicated robustly during elongation (18). As a detailed molecular picture, the dock-lock model has been provided (19). On the other hand, cross-seeding is less likely to proceed than self-seeding, although it occurs when proteins can cross a species barrier, as seen between variants of the same protein (20–22), and, additionally, between heterologous proteins in some cases (23,24). Several studies about the propagation of amyloid structures in cross-seeding have been conducted so far, and in an early report on prion protein variants by Jones and Surewicz, it was demonstrated that the morphology and secondary structure of seed fibrils were inherited exactly when they were used as a template in the cross-seeding of proteins from other species (20). In contrast, recent studies have revealed that cross-seeding sometimes produced amyloid fibrils different from those used as seeds with respect to secondary structure and cytotoxicity (25–27). The latter observations suggest that the complete replication of seed fibrils is not always achieved in cross-seeding, although detailed mechanisms remain unclear.

In this study, we investigated self- and cross-seeding of human and bovine insulin. Insulin is a hormone protein associated with glucose metabolism and consists of two polypeptide chains, the A chain (21 residues) and B chain (30 residues), which are cross-linked by two interchain disulfide bonds. It is one of the best models for studying amyloid formation mechanism because it forms amyloid fibrils readily in vitro (28). Between human and bovine insulin, amino acid sequences differ in three residues (two in the A chain and one in the B chain) (Fig. 1 *A*), whereas their native structures are almost the same (21). Because these amino acid sequences are close enough to cross species barriers with each other, they are good models for investigating interspecies cross-seeding. We tracked preservation or change of amyloid fibril structure in the process of repetitive self- or cross-seeding of human and bovine insulin by using thioflavin T (ThT) fluorescence, atomic force microscopy (AFM), Fourier transform infrared (FTIR) spectroscopy, and iodine staining. In addition, the cytotoxicity of amyloid fibrils was also analyzed using cell lines as one of the indicators of phenotype.

The results of the measurements with several different techniques have demonstrated that human and bovine insulin amyloid fibrils adopted different structures, even though only three residues are different. Although both of these amyloid structures were replicated by self-seeding, they changed gradually when cross-seeding was performed. Notably, a new-type fibril structure with distinct morphology and cytotoxicity was observed when human insulin was cross-seeded with bovine insulin seeds. Here, iodine staining, a coloring reaction through the formation of polyiodide ions on the surface of amyloid fibrils (29), worked as a sensitive probe for reporting changes in amyloid structures. The ultraviolet-visible (UV-Vis) absorption spectra of iodine-stained amyloid fibrils showed complicated changes, and by introducing singular value decomposition (SVD) analysis, intermediate metastable states have been identified in the process of cross-seeding.

MATERIALS AND METHODS

Materials

Recombinant human insulin was purchased form Wako Pure Chemical Industries (Osaka, Japan). Bovine insulin was purchased from Sigma-Aldrich (St. Louis, MO). Iodine, potassium iodine, and ThT were purchased from Wako Pure Chemical Industries. HCl solution and NaCl were purchased from Nacalai Tesque (Kyoto, Japan).

Formation of insulin amyloid fibrils

Human and bovine insulin were dissolved in 25 mM HCl and their concentrations were determined using an absorption coefficient of 1.08 cm^{-1} $(mg/mL)^{-1}$ at 276 nm (30). Spontaneous fibrillation of human and bovine insulin was performed by heating; a sample solution containing 2.0 mg/mL insulin, 25 mM HCl, and 100 mM NaCl was incubated at 65°C for 24 h without agitation. For seeding experiments, seeds were obtained by sonicating preformed fibrils with 20 pulses with 1-s pulse length at a power level of 2.0 W. Seeding reaction was performed under essentially the same solvent conditions as used for the spontaneous fibrillation, except for the addition of 5% (v/v) seeds. The reaction temperature was set at 37°C to prevent spontaneous fibrillation of native insulin, and the incubation time was set for 18 h for each reaction.

ThT fluorescence assay

To assay the formation of amyloid fibrils, a ThT fluorescence assay was performed with fundamentally the same protocol as previously reported (31). In the assay, 3 μL of a sample solution was mixed with 1.5 mL of 5 μM ThT in 50 mM Gly-NaOH buffer (pH 8.5). After 1-min incubation, ThT fluorescence intensity at 485 nm was measured using an excitation wavelength of 445 nm with an RF-5300PC spectrofluorometer (Shimadzu, Kyoto, Japan).

Attenuated total reflectance-FTIR spectroscopy

Attenuated total reflectance (ATR)-FTIR spectra were recorded with a Nicolet iS5 FT-IR equipped with an iD5 ATR accessory (Thermo Fisher

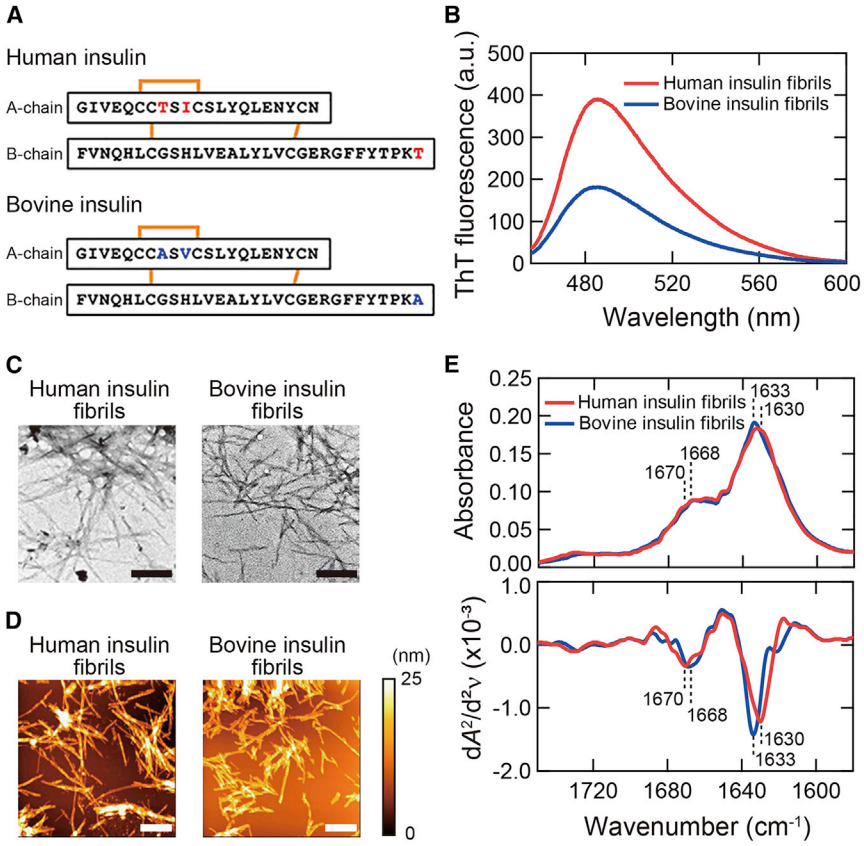

FIGURE 1 Basic properties of human and bovine insulin amyloid fibrils. (*A*) Amino acid sequences of human and bovine insulin. The red and blue characters represent different residues between human and bovine insulin, respectively. (*B*) ThT fluorescence spectra. (*C*) TEM images. The black scale bars represent 200 nm. (*D*) AFM images. The white scale bars represent 1 μm. The color scale on the right represents the height of the sample. (*E*) ATR-FTIR absorption spectra (*upper panel*) and their second derivatives (*lower panel*) in amide I region. The positions of two main peaks of β-sheet and β-turn structures, which were determined from the analysis of local minima of the second derivatives, are indicated on each spectrum. To see this figure in color, go online.

Scientific, Tokyo, Japan). To improve dispersibility, each fibril sample was sonicated before measurements with the same protocol as used for the preparation of seeds. 3.5 μL of a sample solution was spotted onto the surface of a diamond crystal and then dried using compressed air. FTIR spectra were measured by collecting 128 interferograms with a resolution of 4 cm^{-1}. A spectrum of atmospheric air was used as a reference spectrum to subtract the contributions of water vapor and carbon dioxide.

Iodine staining of amyloid fibrils

Iodine staining of amyloid fibrils was performed as previously reported (29). An iodine solution containing 24 mM KI and 3.2 mM I_2 was initially prepared, and each sample of 2.0 mg/mL insulin fibrils was sonicated with the same protocol as used for the preparation of seeds to improve dispersibility. Next, 0.50 mg/mL insulin fibrils containing 0.9 mM KI and 0.12 mM I_2 in 25 mM HCl were prepared by mixing the fibril sample and the iodine solution. After 1-min incubation, the color of the iodine-stained insulin fibrils was analyzed by UV-Vis spectroscopy. UV-Vis absorption spectra were recorded with a JASCO V-650 spectrometer (JASCO, Tokyo, Japan) using a quartz cell with a 1-cm optical length.

AFM

10 μL of a sample solution was loaded to a freshly cleaved mica plate, left for 1 min, then rinsed using 200 μL of distilled water. The residual solution was removed with filter paper and left to dry overnight. AFM images were obtained using a dynamic force mode with Probestation NanoNavi II/IIe (Hitachi High-Tech Science, Tokyo, Japan). The scanning tip used was an OMCL-AC160TS-C3 microcantilever (Olympus, Tokyo, Japan; spring constant equal to 21–37 N/m, resonance frequency equal to 270–340 kHz), and the scan rate was set to 0.5 Hz with the recording of 256 $\times$ 256 points per image.

Transmission electron microscopy

Samples were diluted 10-fold with distilled water, and 5 μL of a sample solution was spotted onto a collodion-coated grid (Nisshin EM, Tokyo, Japan). After 1 min, the solution on the grid was removed with filter paper, then 5 μL of 5% (w/v) hafnium chloride was spotted onto the grid, left for 1 min, and the solution was removed in the same manner. Transmission electron microscopy (TEM) images were obtained using an H-7650 transmission microscope (Hitachi High-Technologies, Tokyo, Japan) with a voltage of 80 kV.

Cytotoxic assay

Cell viability was determined using a 3-(4,5-dimethylthiazol-2-yl)-2,5-diphenyltetrazolium bromide (MTT) Cell Count Kit (Nacalai Tesque, Kyoto, Japan), which is based on the conversion of tetrazolium salt by mitochondrial dehydrogenase to a formazan product. PC12 cells were maintained in Dulbecco's Modified Eagle Medium containing 10% fetal bovine serum, 5% horse serum, penicillin (100 U/mL), and streptomycin (100 μg/mL) in 5% CO_2 at 37°C. The cells were plated in 96-well plates at a density of 20,000 cells per well and grown overnight. The cells were incubated in 110 μL of medium in the absence and presence of insulin samples diluted with phosphate-buffered saline (PBS) to the indicated concentrations. After 24-h incubation, 10 μL of MTT reagents were added and incubated for 4 h in 5% CO_2 at 37°C. The reaction was stopped by adding 100 μL of

solubilization solution (40 mM HCl in 2-propanol). The plates were read with a Multiskan FC microplate reader (Thermo Fisher Scientific, Waltham, MA) at 570 nm. Each sample was assayed in triplicate, and the cell viability was calculated using the value obtained by the addition of PBS alone as a reference.

RESULTS

Formation of human/bovine insulin amyloid fibrils

Human and bovine insulin amyloid fibrils were first prepared by heating under acidic conditions, as used in earlier studies (32–34). After the completion of the reaction, more than 99% of insulin protein was converted to fibrils for both species, which was confirmed by measuring the concentration of residual insulin monomer in the supernatant of the samples after centrifugation. When amyloid fibrils were mixed with ThT, human insulin fibrils showed a higher and slightly red-shifted fluorescence spectrum compared to bovine insulin fibrils (Fig. 1 *B*). In light of the previous suggestion that the ThT fluorescence properties vary depending on the binding mode of ThT on amyloid fibrils (35), the difference in ThT fluorescence spectrum implies that the structures of amyloid fibrils are different between these two species.

We further analyzed the morphology and secondary structure of these amyloid fibrils. TEM images exhibited needle-like morphology in both fibrils, and there was no significant difference in their appearance (Fig. 1 *C*). On the other hand, AFM images revealed a difference in thickness between human (12.5 ± 2.2 nm; $n = 20$) and bovine (7.2 ± 1.4 nm; $n = 20$) insulin fibrils (Fig. 1 *D*). Furthermore, ATR-FTIR spectra in amide I region showed a subtle but significant difference in shape between the two types of insulin fibrils (Fig. 1 *E*; *upper panel*). The second derivative spectra showed the difference more clearly in the wavenumber of minima at around 1630 cm^{-1}, corresponding to β-sheet structure (36), in agreement with the previous report by Surmacz-Chwedoruk et al. (21). In addition, differences in the position of minimum at around 1670 cm^{-1}, corresponding to β-turn (37), were observed (Fig. 1 *E*; *lower panel*). Far-UV CD spectra also showed slightly different spectral shapes between human and bovine insulin fibrils, whereas those in native structure were quite similar (Fig. S1). It was suggested that, whereas both of the human and bovine insulin amyloid fibrils are constructed from cross-β structure in common, there are subtle conformational differences in β-sheet and β-turn.

Color formation of human/bovine insulin amyloid fibrils by iodine staining

We next investigated the color formation of insulin fibrils by iodine staining, whose binding modes have been proposed to vary depending on surface topology of β-pleated sheets and/or their edges (29). The iodine solution itself has yellowish color, showing two major peaks from I_3^- at 288 and 352 nm and a minor broad peak from I_2 at around 425 nm (Fig. S2; (29)). When mixed with an iodine solution, human and bovine insulin fibrils exhibited different colors (Fig. 2 *A*), giving different shapes in the UV-Vis absorption spectra, mainly in a visible region (400–750 nm) (Fig. 2, *B* and *C*). Iodine-stained human insulin fibrils had a major absorption at around 560 nm (Fig. 2 *B*), whereas iodine-stained bovine insulin fibrils had one at around 480 nm (Fig. 2 *C*). This observation indicates that iodine staining can detect differences in fibril structure sensitively. Each specific structure of the human and bovine amyloid fibrils was highly reproducible, which was confirmed by observing quite similar UV-Vis spectra after iodine staining of three independent amyloid fibrils (data not shown).

To evaluate the spectral difference in more detail, we performed spectral deconvolution and compared absorption bands constructing the experimental spectra. Each spectrum was replotted against wavenumber, and spectral deconvolution was performed using a sum of Gaussian distributions according to the following model function:

$$A(\nu) = \sum_{j=1}^{n} A_j \exp\left\{ -\frac{(\nu - \nu_j)^2}{2\sigma_j^2} \right\} \quad (1)$$

where A_j and ν_j represent amplitude and center wavenumber of the jth absorption band, respectively, and σ_j is a coefficient related to the full width at half maximum (FWHM) of the jth absorption band, as is described as $2\sigma_j\sqrt{2\ln 2}$. For stable and accurate convergence, two center wavenumbers and one FWHM of the absorption band parameters were fixed with reference to the local minimum and its distance to the inflection point in the second derivative spectrum.

As a result, the absorption spectra were reproduced with six Gaussians, and the fitted curves reproduced the experimental spectra well (Fig. 2, *D* and *E*). Our previous study revealed that three absorption bands in a higher wavenumber at around 34×10^3, 28×10^3, and 24×10^3 cm^{-1} are assigned to I_3^- and I_2 molecules (*dashed lines* in Fig. 2, *D* and *E*), and the remaining three absorption bands in a lower wavenumber at around 21×10^3, 18×10^3, and 15×10^3 cm^{-1} are assigned to polyiodide ions larger than I_3^- (*filled bands* in Fig. 2, *D* and *E*; (29)). Because the I_3^- and I_2 absorption bands are observed in the iodine solution itself (Fig. S2), the color formation by the iodine staining could be explained by the appearance of the latter three absorption bands, which, in order from the highest wavenumber, we refer to as band I (*orange filled area*), band II (*green filled area*), and band III (*blue filled area*), respectively. The center wavenumbers of the bands I–III were almost the same, but the relative intensity ratio was significantly different between human and bovine insulin fibrils. This observation

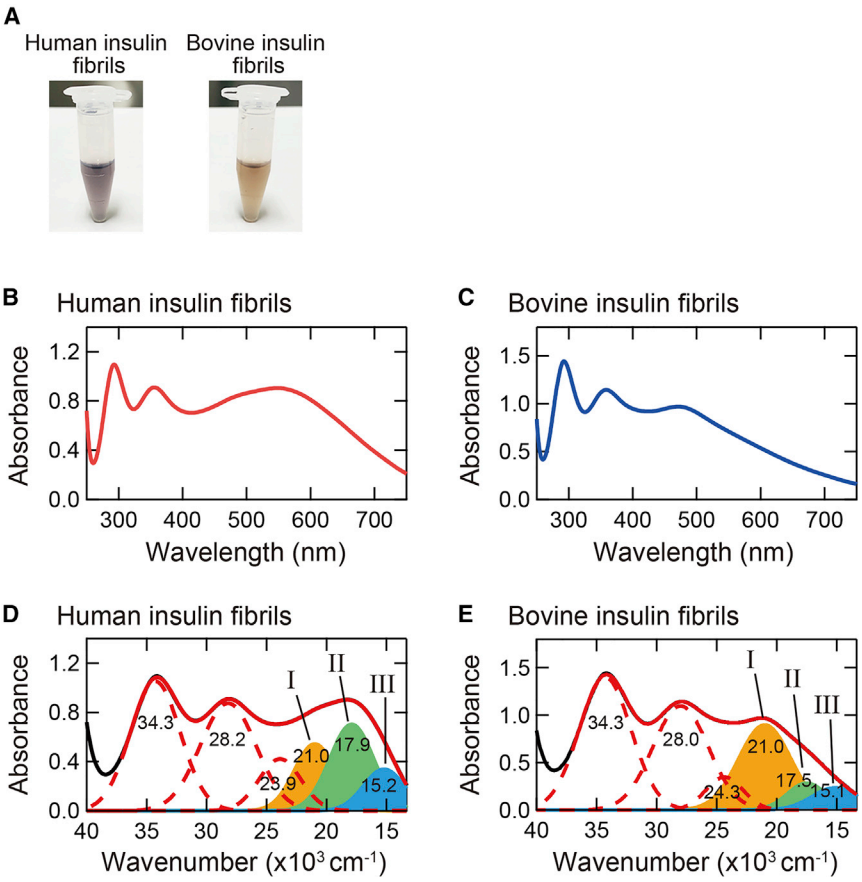

FIGURE 2 Color properties of iodine-stained insulin amyloid fibrils. (*A*) Photographs of iodine-stained human and bovine insulin fibrils. (*B* and *C*) UV-Vis absorption spectra of iodine-stained human (*B*) and bovine (*C*) insulin fibrils. For each absorption spectrum, the spectrum of unstained fibrils was subtracted to obtain net spectrum derived from iodine molecules. (*D* and *E*) Deconvolution of UV-Vis absorption spectra shown in (*B*) and (*C*). Note that the spectra were replotted against wavenumber, and the deconvolution was performed by using Eq. 1. Black and red solid lines represent the experimental and reproduced spectra, respectively, and the experimental spectra are the same as shown in (*B*) and (*C*). Six Gaussian peaks are represented with red dashed lines and filled areas, which correspond to absorption components obtained by the deconvolution. To see this figure in color, go online.

suggests that the constituent iodine binding sites have very similar properties in both insulin fibrils, but the number of binding site and/or the binding constants of polyiodides are different, resulting in different colors.

Structural propagation of insulin amyloid fibrils in self-seeding

We carried out self-seeding experiments to examine the propagation characteristics of amyloid structure. For the seeding reaction, 37°C was selected as reaction temperature to promote only seed-dependent elongation without co-occurrence of the spontaneous fibrillation. The spontaneously formed insulin fibrils analyzed in Figs. 1 and 2 were defined as the first fibrils and used as seeds for the first run of self-seeding reaction. Afterwards, the seeding reactions were repeated using amyloid fibrils of the previous generation as seeds. As a result, ThT fluorescence intensity was preserved, even after the repetitive self-seeding reactions in both species (Fig. 3 *A*), implying each fibril structure was replicated. The first fibrils showed lower intensity than the second–fifth fibrils, which suggests a smaller number or lower affinity of ThT binding, probably because the first fibrils tended to contain diverse fibril morphology (38) and/or fibril clumps with buried surfaces due to the formation at high temperature. However, the results of ATR-FTIR spectra and their second derivatives also showed the preservation of secondary structure, even after the repetitive self-seeding reaction (Fig. 3, *B* and *C*).

The replication of amyloid structure was further verified by iodine staining, which is expected to detect even slight structural differences with high sensitivity (29). The self-seeded second–fifth fibrils consistently exhibited the same shape of UV-Vis absorption spectra throughout all generations (Fig. 3, *D* and *E*), and as a consequence, the spectral deconvolution of the UV-Vis absorption spectra of the fifth fibrils reproduced almost the same absorption bands as those in the first fibrils (Fig. 3, *F* and *G*). The spectral intensity of the first fibrils was slightly lower than those of the second–fifth fibrils, especially in human insulin, although it was not so prominent as that in the case of ThT fluorescence intensity.

Structural propagation of insulin amyloid fibrils in cross-seeding

We further carried out cross-seeding experiments to examine the propagation characteristics of amyloid

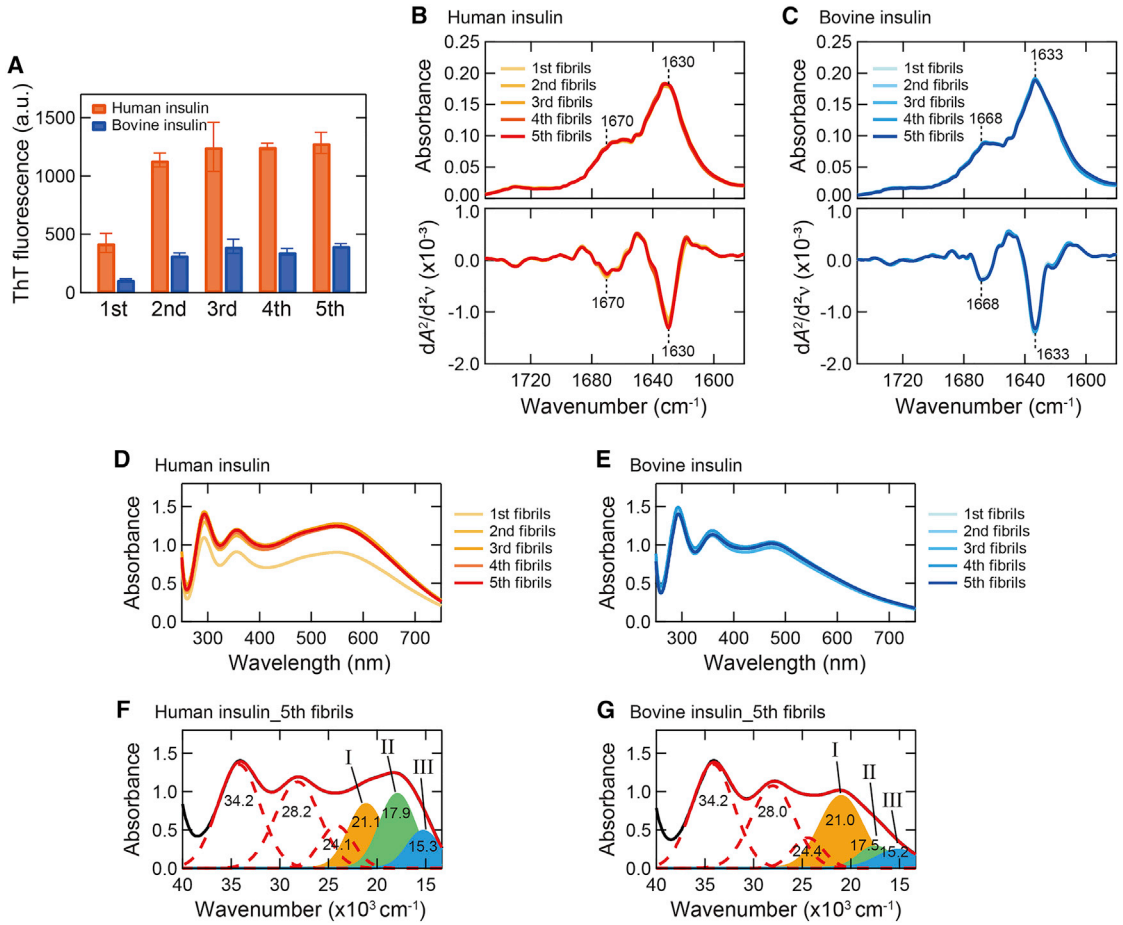

FIGURE 3 Self-seeding of human and bovine insulin. (*A*) ThT fluorescence intensity of the first–fifth amyloid fibrils formed by repeats of self-seeding. The first fibrils correspond to the spontaneously formed amyloid fibrils analyzed in Figs. 1 and 2 and were used as original seeds in this analysis. All samples were assayed in triplicate, and error bars depict standard deviation (SD). (*B* and *C*) ATR-FTIR absorption spectra of the first–fifth amyloid fibrils (*upper panel*) and their second derivatives (*lower panel*) in amide I region of human (*B*) and bovine insulin (*C*). The spectra of the original seeds (i.e., first) are also shown. The positions of two main peaks of β-sheet and β-turn structures are indicated in the graphs. (*D* and *E*) UV-Vis absorption spectra of iodine-stained human (*D*) and bovine insulin fibrils (*E*) formed by self-seeding. For each absorption spectrum, the spectrum of unstained fibrils was subtracted to obtain net spectrum derived from iodine molecules. (*F* and *G*) Deconvolution of UV-Vis absorption spectra of iodine-stained final products (i.e., fifth) of human (*F*) and bovine insulin fibrils (*G*) obtained by self-seeding. To see this figure in color, go online.

structure between proteins with different amino acid sequences. In this work, human/bovine insulin proteins were cross-seeded with bovine/human insulin seeds. For the first cycle of the cross-seeding, the second fibrils obtained in the self-seeding (see Fig. 3) were used as seeds to ensure the structural homogeneity (see Discussion for details), considering that ThT fluorescence intensity and UV-Vis absorption spectrum of the iodine-stained form were smaller in the first fibrils compared with the subsequent generations. As a result, unlike self-seeding, ThT fluorescence intensity of the cross-seeded insulin fibrils gradually changed as generation progressed. Although the first fibrils showed similar intensity to that of the original seeds, ThT fluorescence intensity was gradually decreased in bovine insulin seeded with human insulin seeds, (Fig. 4 *A*, *orange bars*); meanwhile, it was gradually increased in human insulin seeded with bovine insulin seeds (Fig. 4 *A*, *blue bars*). It was suggested that the templating ability of the original seeds is weak upon cross-seeding and thus allows fibril structure to change toward a more thermodynamically stable one.

We next analyzed changes in secondary structure by ATR-FTIR spectroscopy. Similar to the ThT result, the spectra were gradually changed as the reaction was repeated (Fig. 4, *B* and *C*). When bovine insulin was seeded with human seeds, the spectral shape became similar to that of the bovine fibrils (Fig. 4 *B*, see also Fig. 1 *E*), suggesting that the fibril structure changed to the intrinsic fibril structure of bovine insulin. Interestingly, when human insulin was seeded with bovine seeds, the fibril structure did not change to the intrinsic human fibril structure. The spectral shape of the eighth fibrils did not coincide with that of human fibrils, and it showed a deeper second derivative minimum at 1630 cm^{-1} compared with that of human insulin fibrils, and the position of the β-turn shoulder was shifted to

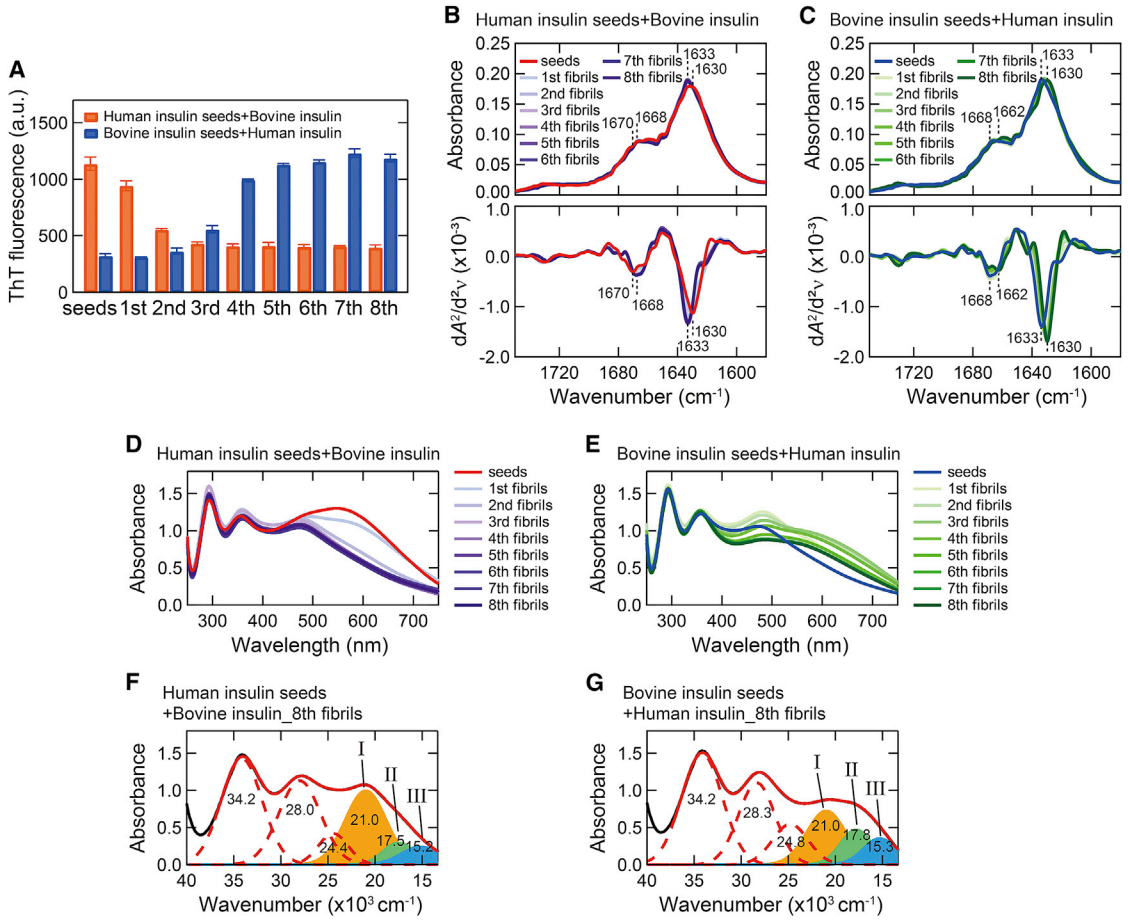

FIGURE 4 Cross-seeding of human and bovine insulin. (*A*) ThT fluorescence intensity of the first–eighth amyloid fibrils. The intensities of the original seeds are also shown. All samples were assayed in triplicate and error bars depict SD. (*B* and *C*) ATR-FTIR absorption spectra of the first–eighth amyloid fibrils (*upper panel*) and their second derivatives (*lower panel*) in amide I region of bovine (*B*) and human insulin (*C*). The spectra of the original seeds are also shown. The positions of two main peaks of β-sheet and β-turn structures are indicated on the spectra of the seed fibrils and the eighth fibrils. (*D* and *E*) UV-Vis absorption spectra of iodine-stained bovine (*D*) and human insulin fibrils (*E*) formed by cross-seeding. (*F* and *G*) Deconvolution of UV-Vis absorption spectra of iodine-stained final products (i.e., eighth) of bovine (*F*) and human insulin (*G*) obtained by cross-seeding. To see this figure in color, go online.

1662 cm^{-1} (Fig. 4 *C*, see also Fig. 1 *E*). It is estimated that a new type of insulin fibrils with distinct β-sheet structure was formed. Far-UV CD analysis also showed a new spectral shape, particularly when human insulin was seeded with bovine seeds (Fig. S3).

We further tracked structural changes during the repeated cross-seeding by using iodine staining. The color of iodine staining detected structural changes successfully, and the UV-Vis absorption spectra of iodine-stained fibrils showed clear spectral changes in a longer wavelength region in both types of cross-seeding (Fig. 4, *D* and *E*). In agreement with the FTIR result, the absorption spectrum reached a distinct shape that was neither human nor bovine fibrils upon seeding of human insulin with bovine seeds, whereas it reached a shape similar to that of the bovine fibrils upon seeding of bovine insulin with human seeds. The spectral deconvolution of the eighth fibrils further verified differences in the composition of the bands I–III from those of the original seeds. When bovine insulin was seeded with human seeds, almost the same component of the absorption bands as those of bovine insulin fibrils was demonstrated (Fig. 4 *F*). When human insulin was seeded with bovine seeds, the relative intensity ratio was clearly different from those of human and bovine fibrils, although the center wavenumbers were similar (Fig. 4 *G*).

Morphology and cytotoxicity of the final fibril product after repeated self-seeding or cross-seeding

To further demonstrate the above-mentioned structural replication or change upon repeated self-seeding or cross-seeding, we performed morphological observation by TEM and AFM and cytotoxic assay. We selected the final generation of insulin fibrils formed by self-seeding (fifth fibrils) and cross-seeding (eighth fibrils) as samples. As a

result, although it was difficult to identify any differences in appearance from TEM images (Fig. 5 *A*), AFM observation successfully revealed the inheritance or change of fibril thickness (Fig. 5 *B*). The thicknesses of self-seeded human and bovine insulin were 12.1 ± 2.0 and 6.9 ± 1.2 nm, respectively ($n = 20$), both of which were almost the same as those of the spontaneously formed human and bovine insulin fibrils. The thicknesses of the cross-seeded human and bovine insulin, on the other hand, were 15.1 ± 1.9 and 6.9 ± 1.3 nm, respectively ($n = 20$). The value of the cross-seeded bovine insulin supports the deviation to bovine-like fibril structure, and the thickest value of the cross-seeded human insulin strongly supports the formation of a new type of fibrils.

We next examined cytotoxicity against PC12 cells by MTT assay. As a result, all of the four types of insulin fibrils showed a decrease in cell viability in a dose-dependent manner (Fig. 5 *C*). The cytotoxicity varied with the type of insulin fibrils, and the self-seeded human insulin yielded significantly lower values of cell viability than the self-seeded bovine insulin (Fig. 5 *C*, *red* and *blue plots*). This result indicates that the different structures of insulin fibrils have different cytotoxicity. The cross-seeded bovine insulin yielded almost the same cytotoxicity as the self-seeded bovine insulin (Fig. 5 *C*, *purple plot*), supporting the formation of bovine-like fibril structure. Interestingly, the cross-seeded human insulin yielded the lowest cell viability that was distinct from human or bovine fibrils (Fig. 5 *C*, *green plot*). This result indicates that the new fibril structure emerged by cross-seeding has a potency to show a new phenotype.

Investigation of the process of the structural changes during the repeated cross-seeding

To gain a detailed picture regarding the pathway of the structural changes induced by cross-seeding, SVD analysis was performed with the UV-Vis absorption spectra of iodine staining in the repeated cross-seeding shown in Fig. 4, *D* and *E*. A set of the UV-Vis spectra, $\boldsymbol{M}$, was decomposed as follows:

$$\boldsymbol{M} = \boldsymbol{U}\boldsymbol{W}\boldsymbol{V}^{\mathbf{T}}, \tag{2}$$

where $\boldsymbol{U}$, $\boldsymbol{W}$, and $\boldsymbol{V}^{\mathbf{T}}$ represent the left-singular matrix, singular matrix, and right-singular matrix of the data set matrix $\boldsymbol{M}$, respectively, assuming that $\boldsymbol{M}$ is an $m \times n$ matrix, $\boldsymbol{U}$ is an $m \times m$ unitary matrix, $\boldsymbol{W}$ is an $m \times n$ diagonal matrix, and $\boldsymbol{V}^{\mathbf{T}}$ is an $n \times n$ unitary matrix. In the analysis, we constructed $\boldsymbol{M}$ containing all the 18 spectra shown in Fig. 4, *D* and *E* in a manner that each column was composed of a single spectrum. In this case, each column of $\boldsymbol{U}$ is interpreted as a normalized diagonalized wave. The weights and proportions of the waves are described by the corresponding diagonal element of $\boldsymbol{W}$, which is called singular values, and corresponding row element of $\boldsymbol{V}^{\mathbf{T}}$, respectively.

As a result, we obtained two dominant singular vectors, the singular values of which satisfied the accumulating contribution ratio of 0.94 (Fig. 6, *A* and *B*). This means that all absorption spectra observed in the cross-seeding are almost reproducible by the sum of the two diagonalized waves multiplied by the proportions. With these singular vectors, which were referred to as SV1 and SV2 in contribution order, we carried out transition diagram analysis by plotting the $\boldsymbol{V}^{\mathbf{T}}$ values of SV1 versus those of SV2. Here, the result of the analysis using the whole wavelength range of the experimental data is shown. The transition diagrams obtained gave curved plots in the both types of cross-seeding, and they were explained by more than one line segment (Fig. 6, *C* and *D*). A single line segment represents a two-state transition, and the points on the line segment can be considered to be a mixture of two fibril structures represented at both ends of the line segment (39,40). The number of the lines thus corresponds to the number of transitions, and the line intersections in the diagrams correspond to intermediate states. The plots in the diagrams were explained by assuming two line segments and one intersection in the cross-seeding of bovine insulin with human insulin seeds

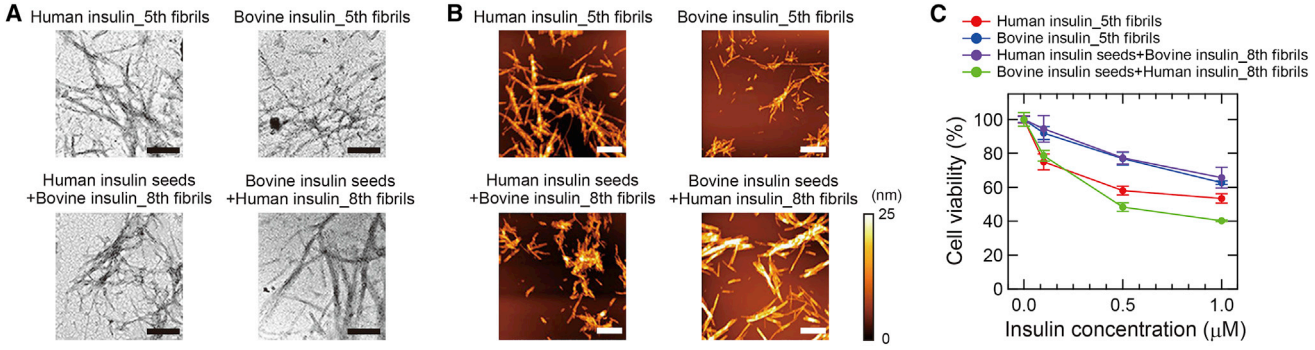

FIGURE 5 Morphology and cytotoxicity of final products of insulin fibrils formed by self- or cross-seeding. (*A*) TEM images. The black scale bars represent 200 nm. (*B*) AFM images. The white scale bars represent 1 μm. The color scale on the right represents the height of the sample. (*C*) Cell viability obtained from MTT assay of insulin fibrils at different concentrations using PC12 cells. Each sample was assayed in triplicate and the error bars depict SD. To see this figure in color, go online.

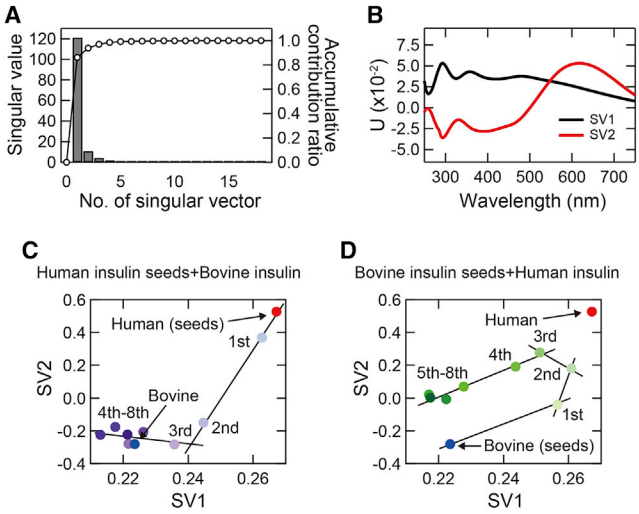

FIGURE 6 SVD analysis of UV-Vis absorption spectra obtained from iodine-stained insulin fibrils formed by cross-seeding. (*A*) The diagonal element of the singular matrix. (*B*) The first (SV1) and second (SV2) columns of the left-singular matrix. (*C* and *D*) Transition diagrams obtained by plotting scores of the first (SV1) and second (SV2) rows of the right-singular matrix. Solid lines, each of which represents a two-state transition, were superimposed to show that both of the plots can be described as a multistep transition. To see this figure in color, go online.

(Fig. 6 *C*) and four linear segments and three intersections in the structural change in cross-seeding of human insulin with bovine insulin seeds (Fig. 6 *D*). These results suggest that these structural changes are multistep, and intermediate metastable states are routed in the process of cross-seeding. The multistep changes were reproduced when another data set of the repeated cross-seeding was subjected to the SVD analysis, although the route did not seem exactly the same in the case of bovine insulin seeded with human seeds (Fig. S4); nevertheless, the plots showed two line segments and finally reached the bovine-type fibril structure, supporting the multistep structural changes in cross-seeding. It was also confirmed that a similar result was obtained even when the wavelength range was limited to 400–750 nm, supporting that spectral changes in the visible region contribute importantly to this analysis.

DISCUSSION

Structural changes induced by cross-seeding of human and bovine insulin

In contrast to exact replication in self-seeding, it was revealed that the cross-seeding of human and bovine insulin caused gradual structural changes from the original seeds. The structural changes occurring in the repeated cross-seeding were successfully tracked by FTIR spectra and iodine staining, and in particular, the changes in visible color of iodine staining were obvious and clearly demonstrated complex changes. Iodine develops color by forming polyiodide ions in complex with crystalline compounds or polymers, and iodine-starch reaction is one of the best-known reactions in which iodine shows blue color by complexing with starch (41). Similarly, amyloid fibrils develop visible color with iodine, which is mechanistically explained by the formation of linear polyiodide ions composed of I_3^- and I_5^- on the fibril surfaces (29,42). Although the use of iodine staining in amyloid researches has not progressed as far, because of the discovery of fluorescent dyes, such as Congo red and ThT, we have recently found that iodine staining could be used as a sensitive probe of structural polymorphism of amyloid fibrils (29). In this study, too, iodine staining worked as a good strategy for evaluating structures of amyloid fibrils and their descendant generations formed by repeated self- or cross-seeding in detail. Considering that different color could be obtained, even when the secondary structure was almost the same as in our previous study, it is expected that the color of iodine staining sensitively senses higher-order structural differences, such as packing of protofilaments.

The most important finding obtained in this study is that the process of the repeated cross-seeding goes through one or more intermediate states. SVD analysis of the UV-Vis spectra obtained from the iodine-stained insulin fibrils revealed structural changes consisting of two or more structural transitions (Fig. 6). Intriguingly, the number and types of intermediates varied depending on the direction of cross-seeding, and furthermore, a new fibril structure with distinct secondary structure, iodine color tones, morphology, and cytotoxicity appeared in a pathway-specific manner when human insulin was cross-seeded with bovine insulin seeds (Figs. 4 and 5). The new fibril structure is not described as a mixture of the intrinsic bovine and human fibril structures because its position in the transition diagram in Fig. 6 *D* is clearly apart from the line connecting the plots of human and bovine fibrils (i.e., *red* and *blue plots*, respectively). The existence of metastable intermediate states is a strong experimental indication of the rugged energy landscape of amyloid fibrils, and the multistep structural changes as well as the pathway dependency of the convergent structure of amyloid fibrils are likely to be a natural consequence arising from the rough energy surface of the amyloid landscape that contains a number of local minima.

Predicted scheme for propagation of amyloid fibrils in cross-seeding

On the basis of these results, we propose a possible scheme of structural propagation induced by self-seeding and cross-seeding of human and bovine insulin. Fig. 7 *A* shows the case of bovine insulin. When bovine insulin is self-seeded, native bovine insulin reaches the inherent bovine-type fibril structure, which is presumed to be the most thermodynamically preferable fibril state of bovine insulin (Fig. 7 *A*, *blue*

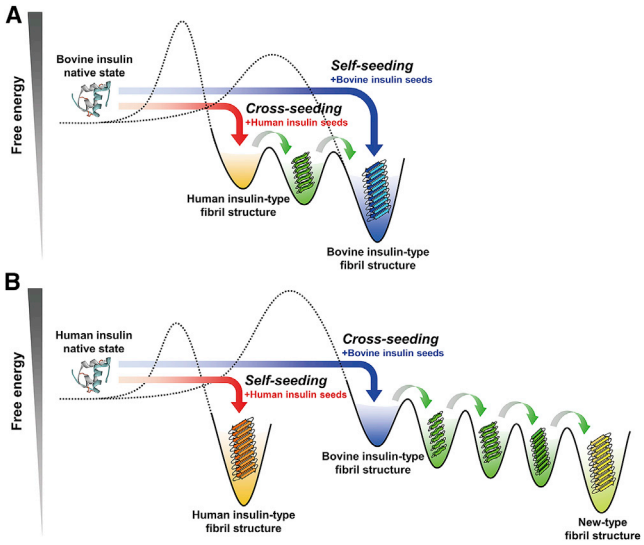

FIGURE 7 Schematic illustration for the energy landscapes of bovine (*A*) and human insulin (*B*). See the main text for details. The number of intermediate states was tentatively determined from the SVD results shown in Fig. 6, *C* and *D*. It should be noted that the energy level of each structural state and the height of each energy barrier in the illustration do not include quantitative information. To see this figure in color, go online.

arrow). In contrast, upon cross-seeding, native bovine insulin first falls into the state of human-type fibril structure by templating with human insulin seeds (Fig. 7 *A*, *red arrow*). However, stepwise structural changes via an intermediate metastable state accompany this, and the fibril structure eventually adapts to the bovine-type fibril structure. Such multistep structural changes in cross-seeding are probably explained by conformational shift of amyloid structures due to the stepwise generation of more thermodynamically advantageous structures by repeated cross-seeding. Here, it should be noted that similar structural transitions may occur through growth competition among different fibrils if initial seeds contain some structural variants (43). However, given that almost no structural change was observed, even after the repetitive self-seeding (Fig. 3), it is indicated that the seeds used for cross-seeding are very homogeneous, although there is some variety at the level of morphology (38). Based on the assurance of the fibril homogeneity from the behavior in the repeated self-seeding as well as the use of the second fibrils, the structural changes in cross-seeding are more likely to have occurred by structural adaptation rather than competition among preexisting fibrils.

In the case of human insulin (Fig. 7 *B*), the energy landscape is predicted to have different features, given that its cross-seeding eventually reaches a new-type fibril structure rather than the inherent human-type fibrils. When human insulin is self-seeded, native human insulin selectively reaches the inherent human-type fibril structure (Fig. 7 *B*, *red arrow*). When cross-seeded with bovine insulin seeds, native human insulin would first fall into the bovine-type fibril structure. However, the structure changes through several intermediate metastable states. Interestingly, unlike the cross-seeding of bovine insulin in Fig. 7 *A*, the pathway leads to the new structure (Fig. 7 *B*, *blue arrow*). The intrinsic human fibril structure is presumed to be kinetically blocked by a large energy barrier, resulting in the observation that human insulin finally took the new-type fibril structure.

Regarding the structural characteristics of the intermediate states and the newly emerged fibril structure, they could not be mentioned only from the results of iodine staining because the relationship between its color tone and the property of amyloid structure still remain unclear (29). To gain insights into the structural characteristics of the intermediates, we attempted SVD of the ATR-FTIR spectra. Although the plots were more scattered than those of iodine staining, the transition diagram in the cross-seeding of human insulin with bovine seeds gave nonlinear shapes of the plots, in agreement with the result of iodine staining (Fig. S5). Additionally, the major peaks were observed in a range of 1620–1640 cm^{-1} in the singular vectors SV1 and SV2, from which it was implicated that the intermediate metastable states result from slight differences in β-sheet conformation. If further studies reveal the relationship between iodine color and amyloid structure, detailed structural characteristics will be clarified.

Implication for the manner of fibril propagation in cross-seeding

From previous studies of prion protein and other proteins, the "conformational selection and population shift" model, which has originally been proposed for explaining biomolecular recognition, has so far been recognized as a valid model to explain the molecular mechanism of cross-seeding (44). In this model, each protein is considered to possess a set of thermodynamically permissible structures, and the overlap of one or more of these structures between proteins with different sequences indicates the achievement of cross-seeding across a species barrier. Indeed, it can explain many experimental observations, including cross-species prion transmission (45) and cross-talk between Aβ42 and Aβ40 (22). When this model is adapted to the energy landscape observed in this study, the thermodynamically permissible structures per protein correspond reasonably to a number of energy minima distributing over the landscape. If any of these energy minima coincide with the seed fibril structure, seed fibrils will interact with the counterprotein molecules and guide them to fall to the energy minimum of the seed structure by skipping the nucleation barrier.

In addition to a large number of energy minima as candidates of fibril structures to be selected, an additional property worth noting is that some energy minima are positioned adjacently on the landscape and tend to connect

mutually by low-energy barriers. This topology allows the deviation of fibril structure, so-called conformational switching, drift, adaptation, or evolution (25,46–48). In such cases, it is not so uncommon for fibrils to take a distinct structure from that of the original seeds as observed in the cross-seeding of this study. Furthermore, it is expected that the energetic pathway to the final state will become rugged with multiple minima, resulting in the transient formation of metastable states. Considering this feature of the energy landscape, multiple cycles of cross-seeding will show dynamic equilibrium with transient accumulation of several different fibril species. If such energetic properties are generalized to a wide range of pathogenic proteins, cross-seeding will produce a variety of fibril structures over a time period of transmission and thus will be involved in pathology in a more complicated manner, causing time-dependent fluctuation in infectivity and pathogenesis.

The energy landscape of amyloid fibrils is thought to vary with protein sequence (10), which will contribute to determining candidates of the final amyloid structure generated by cross-seeding. In addition to this, a specific interaction of protein molecules with seeds is another important factor because it decides an initial landing point on the energy landscape (i.e., fibril templating). To investigate the role of the three different amino acid residues between human and bovine insulin in the latter issue, cross-seeding of human/bovine insulin was assessed using amyloid fibrils consisting of the human A chain or B chain (49,50) as seeds. However, these fibrils did not function as a fibril template, only accelerating fibril formation by shortening induction period (Fig. S6). This result suggests that the interaction between the proteins and seeds is not restricted to local amino acid sequence, but more higher-order and complex factors are involved for exerting template ability.

CONCLUSION

Through this study, a comprehensive understanding of the propagation mechanism of cross-seeding has been progressed from the perspective of the energy landscape. The observation of the multistep structural changes has shed light on molecular details of the conformational deviations and the emergence of a new fibril structure. Remarkably, the presence of the metastable fibril states is a new physicochemical aspect of cross-seeding, and suggests the dynamic feature of amyloid structure during the time course of cross-seeding. The cross-seeding has been reported not only between isoforms of the same protein but also between different proteins, and it is considered to be important for understanding pathology and, furthermore, cross-talk between different amyloid diseases (51–53). Given that heterologous proteins are actually involved in the pathology of several diseases, such as Alzheimer's disease, prion disease, Parkinson's disease, and type 2 diabetes (22,24), accelerating research on cross-seeding will pave new perspectives on the mechanism of pathology at the level of protein molecules.

SUPPORTING MATERIAL

Supporting Material can be found online at https://doi.org/10.1016/j.bpj.2020.12.005.

AUTHOR CONTRIBUTIONS

K.Y. and E.C. designed experiments. K.Y., M.N., M.S., and T.I. performed experiments. K.Y., N.Y., M.T., Y.G., and E.C. performed data analysis. K.Y. and E.C. wrote the manuscript. All authors discussed the results and commented on the manuscript.

ACKNOWLEDGMENTS

This work was performed in part under the Collaborative Research Program of Institute for Protein Research, Osaka University, CR-19-02. This work was supported by the Japan Society for the Promotion of Science Core-to-Core Program, A. Advanced Research Networks. This work was funded by Japan Society for the Promotion of Science KAKENHI, grant numbers JP16H04778, JP17H06352, JP20H03224, and JP20K21396.

REFERENCES

1. Dobson, C. M. 2003. Protein folding and misfolding. *Nature*. 426:884–890.
2. Uversky, V. N., and A. L. Fink. 2004. Conformational constraints for amyloid fibrillation: the importance of being unfolded. *Biochim. Biophys. Acta.* 1698:131–153.
3. Sipe, J. D., M. D. Benson, and P. Westermark. 2014. Nomenclature 2014: amyloid fibril proteins and clinical classification of the amyloidosis. *Amyloid.* 21:221–224.
4. Iadanza, M. G., M. P. Jackson, and S. E. Radford. 2018. A new era for understanding amyloid structures and disease. *Nat. Rev. Mol. Cell Biol.* 19:755–773.
5. Toyama, B. H., and J. S. Weissman. 2011. Amyloid structure: conformational diversity and consequences. *Annu. Rev. Biochem.* 80:557–585.
6. Al-Garawi, Z. S., K. L. Morris, and L. C. Serpell. 2017. The diversity and utility of amyloid fibrils formed by short amyloidogenic peptides. *Interface Focus.* 7:20170027.
7. Li, B., P. Ge, and L. Jiang. 2018. Cryo-EM of full-length α-synuclein reveals fibril polymorphs with a common structural kernel. *Nat. Commun.* 9:3609.
8. Kollmer, M., W. Close, and M. Fändrich. 2019. Cryo-EM structure and polymorphism of Aβ amyloid fibrils purified from Alzheimer's brain tissue. *Nat. Commun.* 10:4760.
9. Tycko, R. 2014. Physical and structural basis for polymorphism in amyloid fibrils. *Protein Sci.* 23:1528–1539.
10. Theint, T., P. S. Nadaud, and C. P. Jaroniec. 2017. Species-dependent structural polymorphism of Y145Stop prion protein amyloid revealed by solid-state NMR spectroscopy. *Nat. Commun.* 8:753.
11. Diaz-Avalos, R., C. Y. King, and D. L. Caspar. 2005. Strain-specific morphologies of yeast prion amyloid fibrils. *Proc. Natl. Acad. Sci. USA.* 102:10165–10170.
12. Zako, T., M. Sakono, and M. Maeda. 2009. Bovine insulin filaments induced by reducing disulfide bonds show a different morphology, secondary structure, and cell toxicity from intact insulin amyloid fibrils. *Biophys. J.* 96:3331–3340.

13. Tanaka, M., P. Chien, and J. S. Weissman. 2004. Conformational variations in an infectious protein determine prion strain differences. *Nature.* 428:323–328.
14. Collinge, J., and A. R. Clarke. 2007. A general model of prion strains and their pathogenicity. *Science.* 318:930–936.
15. Qiang, W., W. M. Yau, and R. Tycko. 2017. Structural variation in amyloid-β fibrils from Alzheimer's disease clinical subtypes. *Nature.* 541:217–221.
16. Falcon, B., W. Zhang, and M. Goedert. 2018. Structures of filaments from Pick's disease reveal a novel tau protein fold. *Nature.* 561:137–140.
17. Jarrett, J. T., and P. T. Lansbury, Jr. 1993. Seeding "one-dimensional crystallization" of amyloid: a pathogenic mechanism in Alzheimer's disease and scrapie? *Cell.* 73:1055–1058.
18. Petkova, A. T., R. D. Leapman, and R. Tycko. 2005. Self-propagating, molecular-level polymorphism in Alzheimer's β-amyloid fibrils. *Science.* 307:262–265.
19. Esler, W. P., E. R. Stimson, and J. E. Maggio. 2000. Alzheimer's disease amyloid propagation by a template-dependent dock-lock mechanism. *Biochemistry.* 39:6288–6295.
20. Jones, E. M., and W. K. Surewicz. 2005. Fibril conformation as the basis of species- and strain-dependent seeding specificity of mammalian prion amyloids. *Cell.* 121:63–72.
21. Surmacz-Chwedoruk, W., H. Nieznańska, and W. Dzwolak. 2012. Cross-seeding of fibrils from two types of insulin induces new amyloid strains. *Biochemistry.* 51:9460–9469.
22. Yoo, B. K., Y. Xiao, and Y. Ishii. 2018. E22G pathogenic mutation of β-amyloid (Aβ) enhances misfolding of Aβ40 by unexpected prion-like cross talk between Aβ42 and Aβ40. *J. Am. Chem. Soc.* 140:2781–2784.
23. O'Nuallain, B., A. D. Williams, and R. Wetzel. 2004. Seeding specificity in amyloid growth induced by heterologous fibrils. *J. Biol. Chem.* 279:17490–17499.
24. Katorcha, E., N. Makarava, and I. V. Baskakov. 2017. Cross-seeding of prions by aggregated α-synuclein leads to transmissible spongiform encephalopathy. *PLoS Pathog.* 13:e1006563.
25. Peretz, D., R. A. Williamson, and M. R. Scott. 2002. A change in the conformation of prions accompanies the emergence of a new prion strain. *Neuron.* 34:921–932.
26. Hu, R., B. Ren, and J. Zheng. 2017. Seed-induced heterogeneous cross-seeding self-assembly of human and rat islet polypeptides. *ACS Omega.* 2:784–792.
27. Hao, X., J. Zheng, and X. Dong. 2019. Seeding and cross-seeding aggregations of Aβ40 and its N-terminal-truncated peptide Aβ11–40. *Langmuir.* 35:2821–2831.
28. Groenning, M., S. Frokjaer, and B. Vestergaard. 2009. Formation mechanism of insulin fibrils and structural aspects of the insulin fibrillation process. *Curr. Protein Pept. Sci.* 10:509–528.
29. Hiramatsu, T., N. Yamamoto, and E. Chatani. 2020. Iodine staining as a useful probe for distinguishing insulin amyloid polymorphs. *Sci. Rep.* 10:16741.
30. Nielsen, L., R. Khurana, and A. L. Fink. 2001. Effect of environmental factors on the kinetics of insulin fibril formation: elucidation of the molecular mechanism. *Biochemistry.* 40:6036–6046.
31. Naiki, H., K. Higuchi, and T. Takeda. 1989. Fluorometric determination of amyloid fibrils in vitro using the fluorescent dye, thioflavin T1. *Anal. Biochem.* 177:244–249.
32. Waugh, D. F. 1946. A fibrous modification of insulin. I. The heat precipitate of insulin. *J. Am. Chem. Soc.* 68:247–250.
33. Brange, J., L. Andersen, and E. Rasmussen. 1997. Toward understanding insulin fibrillation. *J. Pharm. Sci.* 86:517–525.
34. Whittingham, J. L., D. J. Scott, and G. Guy Dodson. 2002. Insulin at pH 2: structural analysis of the conditions promoting insulin fibre formation. *J. Mol. Biol.* 318:479–490.
35. Groenning, M. 2010. Binding mode of Thioflavin T and other molecular probes in the context of amyloid fibrils-current status. *J. Chem. Biol.* 3:1–18.
36. Krimm, S., and J. Bandekar. 1986. Vibrational spectroscopy and conformation of peptides, polypeptides, and proteins. *Adv. Protein Chem.* 38:181–364.
37. Bandekar, J. 1992. Amide modes and protein conformation. *Biochim. Biophys. Acta.* 1120:123–143.
38. Jiménez, J. L., E. J. Nettleton, and H. R. Saibil. 2002. The protofilament structure of insulin amyloid fibrils. *Proc. Natl. Acad. Sci. USA.* 99:9196–9201.
39. Uversky, V. N., L. N. Garriques, and A. L. Fink. 2003. Prediction of the association state of insulin using spectral parameters. *J. Pharm. Sci.* 92:847–858.
40. Ahmad, A., I. S. Millett, and A. L. Fink. 2003. Partially folded intermediates in insulin fibrillation. *Biochemistry.* 42:11404–11416.
41. Okuda, M., T. Hiramatsu, and E. Chatani. 2020. Theoretical modeling of electronic structures of polyiodide species included in α-cyclodextrin. *J. Phys. Chem. B.* 124:4089–4096.
42. Dzwolak, W. 2007. Insulin amyloid fibrils form an inclusion complex with molecular iodine: a misfolded protein as a nanoscale scaffold. *Biochemistry.* 46:1568–1572.
43. Kihara, M., E. Chatani, and Y. Goto. 2005. Seeding-dependent maturation of β_2-microglobulin amyloid fibrils at neutral pH. *J. Biol. Chem.* 280:12012–12018.
44. Ma, B., and R. Nussinov. 2012. Selective molecular recognition in amyloid growth and transmission and cross-species barriers. *J. Mol. Biol.* 421:172–184.
45. Tanaka, M., P. Chien, and J. S. Weissman. 2005. Mechanism of cross-species prion transmission: an infectious conformation compatible with two highly divergent yeast prion proteins. *Cell.* 121:49–62.
46. Makarava, N., V. G. Ostapchenko, and I. V. Baskakov. 2009. Conformational switching within individual amyloid fibrils. *J. Biol. Chem.* 284:14386–14395.
47. Surmacz-Chwedoruk, W., V. Babenko, and W. Dzwolak. 2016. The emergence of superstructural order in insulin amyloid fibrils upon multiple rounds of self-seeding. *Sci. Rep.* 6:32022.
48. Wang, Y., and C. K. Hall. 2018. Seeding and cross-seeding fibrillation of N-terminal prion protein peptides PrP(120-144). *Protein Sci.* 27:1304–1313.
49. Hong, D. P., A. Ahmad, and A. L. Fink. 2006. Fibrillation of human insulin A and B chains. *Biochemistry.* 45:9342–9353.
50. Yamamoto, N., S. Tsuhara, and E. Chatani. 2018. A specific form of prefibrillar aggregates that functions as a precursor of amyloid nucleation. *Sci. Rep.* 8:62.
51. Morales, R., I. Moreno-Gonzalez, and C. Soto. 2013. Cross-seeding of misfolded proteins: implications for etiology and pathogenesis of protein misfolding diseases. *PLoS Pathog.* 9:e1003537.
52. Chaudhuri, P., K. P. Prajapati, and K. Kar. 2019. Amyloid cross-seeding raises new dimensions to understanding of amyloidogenesis mechanism. *Ageing Res. Rev.* 56:100937.
53. Ren, B., Y. Zhang, and J. Zheng. 2019. Fundamentals of cross-seeding of amyloid proteins: an introduction. *J. Mater. Chem. B Mater. Biol. Med.* 7:7267–7282.

Biophysical Journal, Volume *120*

Supplemental Information

Multistep Changes in Amyloid Structure Induced by Cross-Seeding on a Rugged Energy Landscape

Keisuke Yuzu, Naoki Yamamoto, Masahiro Noji, Masatomo So, Yuji Goto, Tetsushi Iwasaki, Motonari Tsubaki, and Eri Chatani

Supplemental Methods

CD spectroscopy.

CD spectra were recorded using a J-1100 spectropolarimeter (JASCO, Tokyo, Japan). Sample solutions were prepared at a protein concentration of 0.2 mg/mL in 25 mM HCl for native insulin and 0.2 mg/mL in 25 mM HCl containing 100 mM NaCl for fibril samples, and in the measurement of amyloid fibrils, the sample was sonicated to improve dispersibility. Each scan was performed at 20 nm/min from 250 to 196 nm with a 0.1 cm path-length quartz cell. All spectra were obtained from the integration of five individual scans and expressed as mean residue molar ellipticity [θ] in monomer unit.

Purification of A-chain and B-chain.

A-chain and B-chain were obtained from human insulin. A-chain was purified as described previously (1) with a slight modification. Human insulin was dissolved at a concentration of 5.0 mg/mL in 50 mM sodium phosphate buffer (pH 7.4) containing 1 mM ethylenediaminetetraacetic acid and 10 mM dithiothreitol. After overnight incubation at 25 °C, the solution was centrifuged at 1,800 ×g for 30 min and A-chain in the supernatant was separated, and then solvent exchange with Milli-Q water was performed using a PD-10 column. B-chain was purified as described in our previous report (2). The A-chain and B-chain concentrations were determined using absorption coefficients of 1.07 $(mg/mL)^{-1}$ cm^{-1} and 0.90 $(mg/mL)^{-1}$ cm^{-1} at 280 nm (1, 2), respectively.

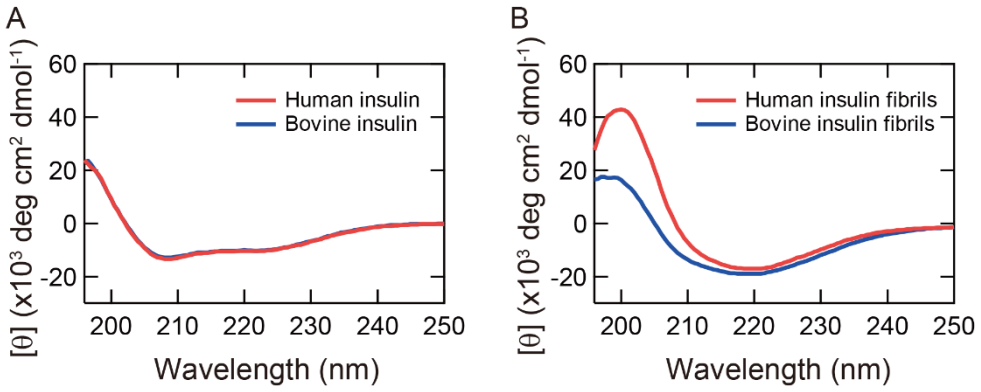

Figure S1. Far-UV CD spectra of human and bovine insulin in (A) native and (B) fibrillar states. In panel B, the same amyloid fibrils investigated in Figure 1 were subjected to the CD measurements.

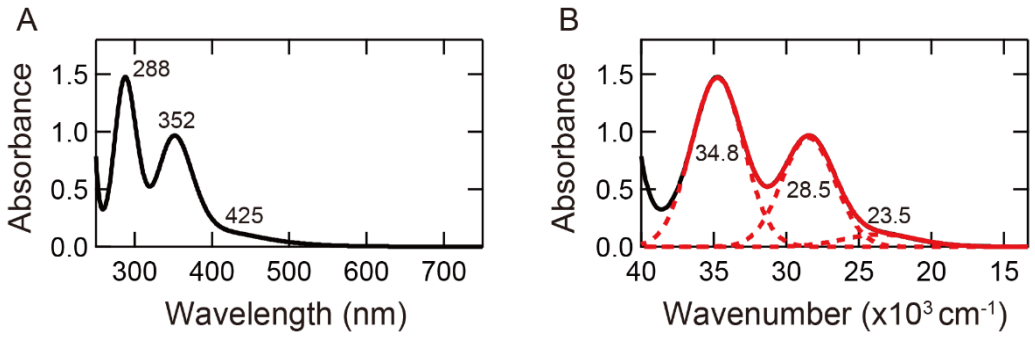

Figure S2. UV-Vis spectrum (A) and its deconvolution (B) of an iodine solution. An iodine solution containing 0.9 mM KI and 0.12 mM I_2 in 25 mM HCl was used for the measurement. A black line represents the experimental spectrum, and a red line represents the fitted spectrum using eq. 1 assuming three Gaussian bands (i.e., $n = 3$). Three Gaussian peaks are represented with dashed red lines, which correspond to absorption components obtained by the deconvolution. The Gaussian bands at 288 nm (35×10^3 cm^{-1}) and 352 nm (29×10^3 cm^{-1}) were assigned to I_3^-, and that at 425 nm (24×10^3 cm^{-1}) was assigned to I_2 (3).

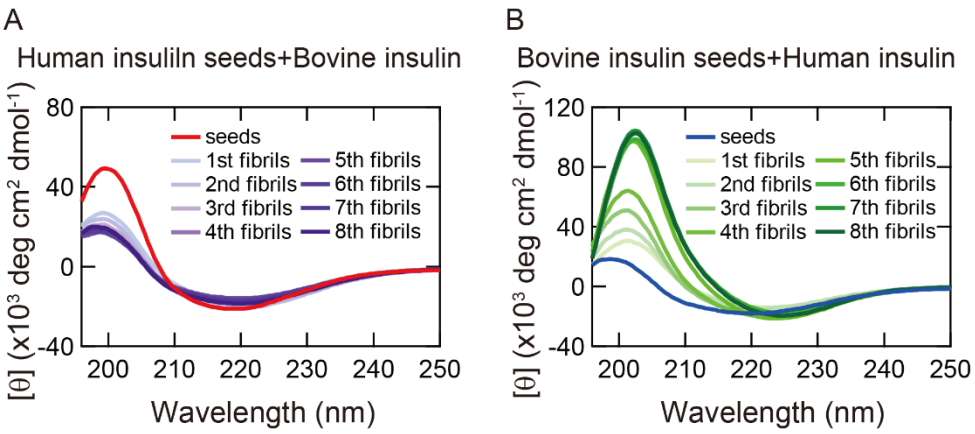

Figure S3. Far-UV CD spectra of (A) bovine insulin cross-seeded with human seeds and (B) human insulin cross-seeded with bovine seeds. The same amyloid fibrils investigated in Figure 4 were subjected to the CD measurements.

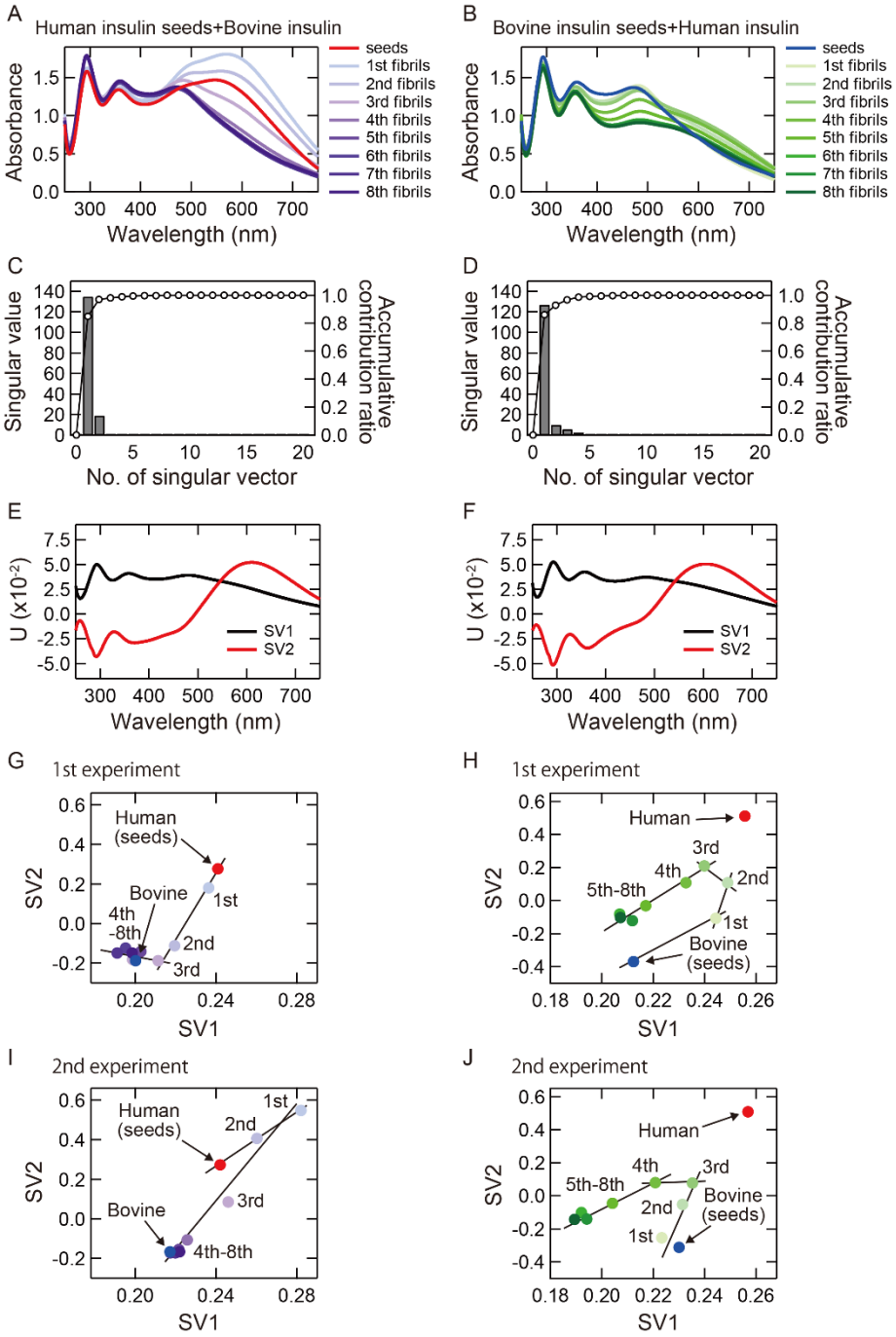

Figure S4. Reproducibility of SVD analysis of UV-Vis absorption spectra obtained from iodine-stained insulin fibrils formed by cross-seeding. To examine the reproducibility of the placement of points and the line segments on the SVD diagram, an additional SVD analysis was performed for each type of cross-seeding using a newly obtained dataset in addition to the original one. (A, B) UV-Vis absorption spectra of iodine-stained bovine (A) and human insulin fibrils (B) formed by cross-seeding. The datasets in panels A and B, respectively were subjected to SVD analysis together with the original ones shown in Figure 4D, E, respectively. Before the analysis, the intensity of the two independent datasets was normalized based on the peak intensity around 295 nm

of the seeds. (C, D) The diagonal element of the singular matrix for the datasets of bovine insulin seeded with human seeds (C) and those of human insulin seeded with bovine seeds (D). (E, F) The 1st (SV1) and 2nd (SV2) columns of the left-singular matrix of bovine insulin seeded with human seeds (E) and human insulin seeded with bovine seeds (F). Both of the results showed two dominant singular vectors SV1 and SV2 similar to those shown in Figure 6B. (G-J) Transition diagrams obtained by plotting scores of the 1st (SV1) and 2nd (SV2) rows of the right-singular matrix of bovine insulin seeded with human seeds (G, I) and human insulin seeded with bovine seeds (H, J). Solid lines were superimposed in all panels to estimate the number of transitions.

As shown in panels H and J, the transition diagram of human insulin seeded with bovine seeds successfully reproduced the characteristic U-shaped route with similar placements of the plots, and the formation of the same new-type fibrils was also confirmed. However, regarding the number of line segments, only three line segments were identified in panel J and it was difficult to conclude the exact number of intermediate metastable states that pass through during the cross-seeding process.

In the case of bovine insulin seeded with human seeds, significant differences in the placement of the plots were observed between panels G and I, failing to reproduce the same route of the structural transitions. Nevertheless, the plots were composed of two line segments. It was also demonstrated that fibril structure changed to the intrinsic fibril structure of bovine insulin after multistep structural changes. Although the pathways were diverse, it was finally concluded that the structural changes proceed with a two-step structural transition through an intermediate metastable state.

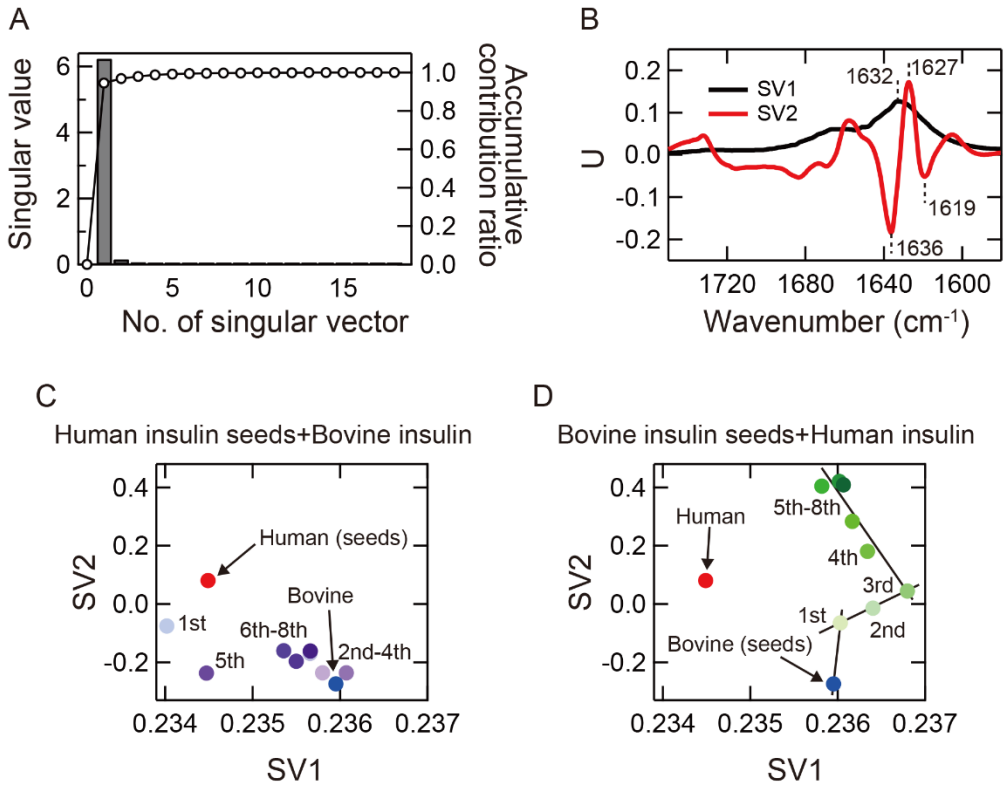

Figure S5. SVD analysis of ATR-FTIR spectra obtained from insulin fibrils formed by cross-seeding. The SVD analysis was performed with the FTIR spectra observed in the repeated cross-seeding shown in Figure 4B, C. (A) The diagonal element of the singular matrix. (B) The 1st (SV1) and 2nd (SV2) columns of the left-singular matrix. The positions of main peaks at around 1630 cm^{-1} indicative of β-sheet structures are labeled in the graphs. (C, D) Transition diagrams obtained by plotting scores of the 1st (SV1) and 2nd (SV2) rows of the right-singular matrix. The plots in the transition diagrams were more scattered than those of iodine staining due to small changes in FTIR spectra, making it relatively difficult to capture intermediate states especially in the cross-seeding of bovine insulin with human seeds (C). Nevertheless, the transition diagram of the cross-seeding of human insulin with bovine seeds showed systematic changes in plots which could be represented by the combination of multiple linear segments (D). In this plot, the most of the intermediates identified in Figure 6 were found, except for one in the 1st–3rd generations. The partial success in the SVD analysis of the FTIR spectra suggests that the multistep structural transitions could also be detected at the secondary structure level. It is tempting to find a clear correlation in singular vectors between FTIR spectra and iodine staining; however, this could not be achieved only with the present experimental data.

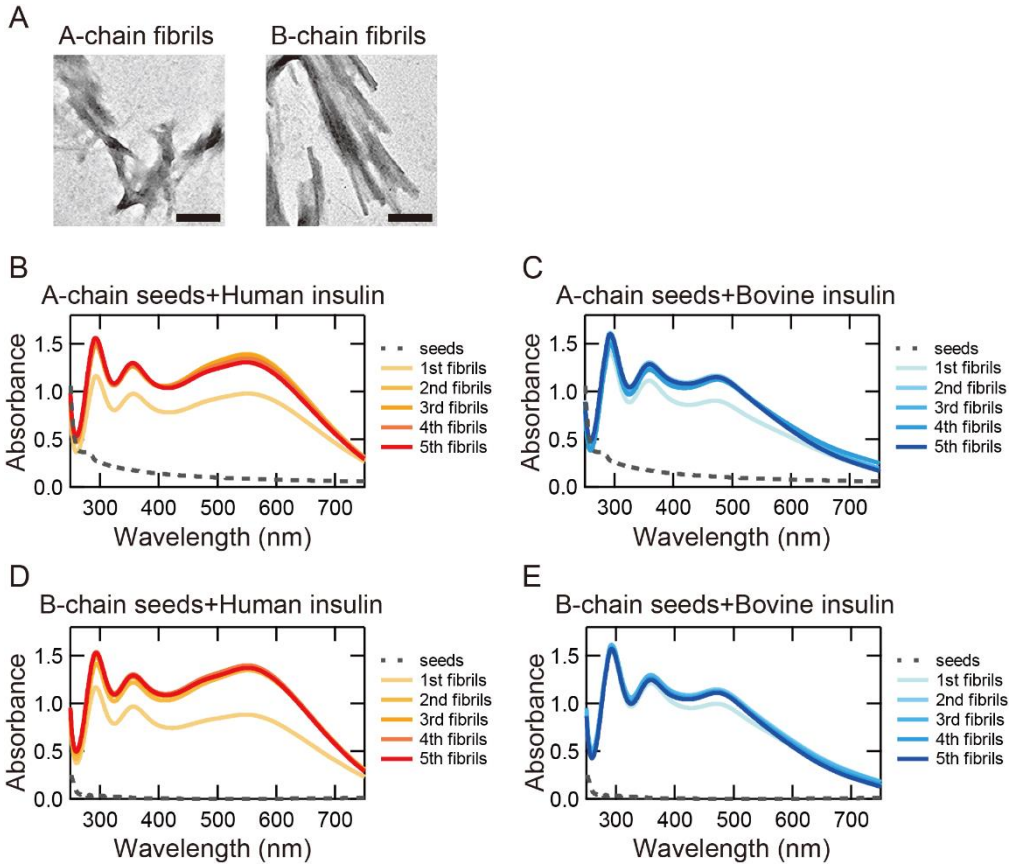

Figure S6. Cross-seeing of human/bovine insulin using human A-chain and B-chain fibrils as seeds. (A, B) TEM images of A-chain (A) and B-chain fibrils (B). The black scale bars represent 200 nm. (C–F) UV-Vis absorption spectra of iodine-stained human and bovine insulin cross-seeded with A-chain (C, D) or B-chain fibrils (E, F). Seeding reaction was performed under the same conditions as used for the cross-seeding with human or bovine insulin fibrils as seeds in Figure 4. The incubation time was set to 18 h for each cycle of cross-seeding except for the first cycle, where the incubation time was changed to 100 h because the reaction speed was much slower. Iodine staining was performed by using the same protocols as used for the self- and cross-seeding with human or bovine insulin fibrils as seeds in Figures 3 and 4. As shown by dashed lines in (C) and (D), A-chain and B-chain fibrils themselves showed little absorption even after mixing with iodine solution, probably due to the disruption of polyiodide ions by their reduction by free thiol groups of cysteine residues in A-chain and B-chain fibrils. The UV-Vis absorption spectra showed a similar shape to those of the self-seeding of human and bovine insulin, respectively (see Figure 3D, E), demonstrating that A-chain and B-chain fibrils did not work as a template.

Supporting References

1. Hong, D. P., A. Ahmad, and A. L. Fink. 2006. Fibrillation of human insulin A and B chains. *Biochemistry.* 45:9342-9353.
2. Yamamoto, N., S. Tsuhara, A. Tamura, and E. Chatani. 2018. A specific form of prefibrillar aggregates that functions as a precursor of amyloid nucleation. *Sci. Rep.* 8:62.
3. Hiramatsu, T., N. Yamamoto, S. Ha, Y. Masuda, M. Yasuda, M. Ishigaki, K. Yuzu, Y. Ozaki, and E. Chatani. 2020. Iodine staining as a useful probe for distinguishing amyloid fibril polymorphs. *Sci. Rep.* 10:16741